Anderson model out of equilibrium: Noncrossing-approximation approach to transport through a quantum dot

Ned S. Wingreen
NEC Research Institute, 4 Independence Way, Princeton, New Jersey 08540

Yigal Meir
Department of Physics, University of California, Santa Barbara, California 93106
(Received 28 September 1993)

The infinite-U Anderson model is applied to transport through a quantum dot. The current and density of states are obtained via the noncrossing approximation for two spin-degenerate levels weakly coupled to two leads. At low temperatures, the Kondo peak in the equilibrium density of states strongly enhances the linear-response conductance. Application of a finite voltage bias reduces the conductance and splits the peak in the density of states. The split peaks, one at each chemical potential, are suppressed in amplitude by a finite dissipative lifetime. We estimate this lifetime perturbatively as the time to transfer an electron from the higher-chemical-potential lead to the lower-chemical-potential one. At zero magnetic field, the clearest signatures of the Kondo effect in transport through a quantum dot are the broadening, shift, and enhancement of the linear-response conductance peaks at low temperatures, and a peak in the nonlinear differential conductance around zero bias.

I. INTRODUCTION

The Kondo effect has been a focus of condensed-matter research for many years. Its essence—the crossover from weak to strong coupling between a magnetic impurity and a conduction-electron sea as temperature is lowered—has inspired both theory and experiment. While most aspects of the problem are now well understood, studies have traditionally been confined to *equilibrium* properties.[1] For the case of a magnetic atom embedded in a bulk metal, achieving nonequilibrium may be daunting, but it is not in the case of "artificial atoms."[2] In particular, we predict that a quantum dot weakly coupled to its leads is a Kondo system in which nonequilibrium can be routinely achieved.[3,4] More generally, an impurity or defect level in a small structure where the applied bias is dropped over a mesoscopic length[5,6] will be a nonequilibrium Kondo system.

Anderson's model[7] for a Kondo impurity—a site with discrete, interacting levels coupled to a band—has already been used successfully to describe experiments on quantum dots.[8–10] The discrete spectrum of a single dot has been observed by transport[11–13] and capacitance[14] spectroscopy, while the strong on-site Coulomb interaction is recognized[15] as the origin of periodic conductance oscillations.[12,13,16] However, it is only the high-temperature regime that has been explored experimentally, while it is at low temperatures that the Kondo effect emerges.

Since the Anderson Hamiltonian describes the quantum dot, at low temperatures the dot must behave as a Kondo impurity. In fact, Glazman and Raikh[17] and Ng and Lee[18] have argued that at zero-temperature equilibrium the Kondo resonance in the density of states of spin-degenerate levels will produce perfect transparency of a quantum dot symmetrically coupled to its leads. More precisely, for all chemical potentials between ϵ_0 and ϵ_0+U, where ϵ_0 is the bare-level energy and U is the interaction energy (Fig. 1), the dot will have the conductance of an open channel, $2e^2/h$. This is to be contrasted with the situation at temperatures larger than Γ, the elastic width of the levels, where the conductance consists of two resonances, at ϵ_0 and at ϵ_0+U. Since the chemical potential of a quantum dot can effectively be swept by changing the voltage on a nearby gate, the Kondo effect will have a striking experimental signature in low-temperature transport through a quantum dot.

Until now, however, only qualitative predictions have been made for experimental observation of the Kondo effect in transport through a quantum dot. Specifically,

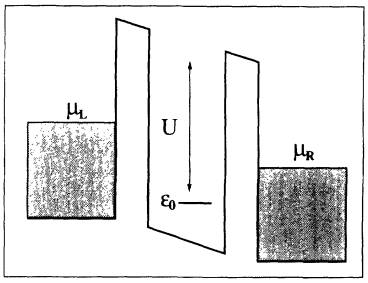

FIG. 1. Schematic band diagram of a quantum dot coupled via tunneling barriers to two leads with different chemical potentials. At zero magnetic field, the energy level ϵ_0 on the quantum dot will be spin degenerate, and a large Coulomb interaction energy U will prevent double occupancy.

raising the temperature above the relevant Kondo temperature is predicted to suppress the peak in the density of states, and, consequently, reduce the conductance.[17,18] As the Kondo temperature near the conductance peak at ϵ_0 depends exponentially on the chemical potential, $T_K(\mu)\sim\exp[-\pi(\mu-\epsilon_0)/\Gamma]$, one expects that the Kondo effect will enhance the conductance mainly for $\epsilon_0<\mu\lesssim\epsilon_0+$few Γ. Accordingly, Ng and Lee[18] predicted that the finite-temperature conductance vs gate voltage will consist of pairs of asymmetric peaks,[19] separated by the Coulomb-interaction energy U. In this work we present a quantitative calculation of the line shape of these conductance peaks, via the noncrossing approximation.[20] We show that at experimentally accessible temperatures the Kondo effect will leave the conductance peaks symmetric. The Kondo effect will manifest itself, instead, in the broadening of the peaks, the enhancement of their amplitude, and the shift in their positions towards each other (for each spin-degenerate pair), as the temperature decreases.

Furthermore, as the leads coupled to a quantum dot are easily biased to nonequilibrium, new physical questions which were not relevant to magnetic impurities can also be raised. In particular, what happens to the Kondo effect out of equilibrium?[3,4] Since at equilibrium the Kondo peak in the density of states occurs at the chemical potential, the presence in nonequilibrium of *two* chemical potentials must have a dramatic effect.

In this paper we try to answer the question of what new behavior is present in the Anderson model out of equilibrium, and to make quantitative predictions for experiment. Generalizing the noncrossing approximation to nonequilibrium, using the Keldysh formalism, we find that a voltage bias between the left and right leads causes the Kondo peak in the density of states to split, leaving a peak in the density of states at the chemical potential of each lead (see Fig. 5 below). The amplitudes of these split peaks are suppressed by a finite nonequilibrium lifetime, due to dissipative transitions in which electrons are transferred from the higher-chemical-potential lead to the lower-chemical-potential one. The narrowness of the Kondo peak in the density of states, and its splitting and suppression, lead to a rapid decrease of conductance with increasing bias. The resulting peak in the nonlinear differential conductance is likely to be the most accessible experimental signature of the Kondo effect in quantum dots.

We begin this paper with a general formulation of nonequilibrium transport through an Anderson impurity in the limit of an infinite on-site interaction energy U (Sec. II A). Short discussions of the mapping into a slave-boson Hamiltonian and of the Keldysh formalism are presented. The noncrossing approximation is then introduced (Sec. II B) and the numerical methods outlined (Sec. II C). Results of the noncrossing approximation are presented for both equilibrium and nonequilibrium transport (Sec. II D). The theoretical interpretation of the results is discussed (Sec. III A) as well as the implications for experiment (Sec. III B). An appendix is included to demonstrate the current-conserving property of the noncrossing approximation.

II. THE NONEQUILIBRIUM ANDERSON MODEL

A. General formulation

1. The model

We model the quantum dot and its leads by the Anderson Hamiltonian[7]

$$H=\sum_{\sigma;k\in L,R}\epsilon_{k\sigma}c^{\dagger}_{k\sigma}c_{k\sigma}+\sum_{\sigma}\epsilon_{\sigma}c^{\dagger}_{\sigma}c_{\sigma}+\tfrac{1}{2}U\sum_{\sigma}\sum_{\sigma'\neq\sigma}n_{\sigma}n_{\sigma'}+\sum_{\sigma;k\in L,R}(V_{k\sigma}c^{\dagger}_{k\sigma}c_{\sigma}+\text{H.c.})\,, \tag{1}$$

where $c^{\dagger}_{k\sigma}$ ($c_{k\sigma}$) creates (destroys) an electron with momentum k and spin σ in one of the two leads, and $c^{\dagger}_{\sigma}$ (c_{σ}) creates (destroys) a spin-σ electron on the quantum dot. The spin quantum number σ may also represent orbital degeneracies as in the magnetic-impurity problem,[7] though, experimentally, these degeneracies are likely to be lifted by disorder in quantum dots. In the following we will focus on spin-degenerate states. The third term describes the Coulomb interaction among electrons on the dot. We assume that $U\to\infty$, forbidding double occupancy. This is appropriate for quantum dots where, typically, U ($\sim$1 meV) is a hundred times larger than the coupling to the leads[21] Γ ($\sim$10 μeV). The fourth term describes the hopping between the leads and the dot, and determines this coupling strength via

$$\Gamma^{L(R)}_{\sigma}(\omega)=2\pi\sum_{k\in L(R)}|V_{k\sigma}|^2\delta(\omega-\epsilon_{k\sigma})\,. \tag{2}$$

Our aim is to calculate the current through the quantum dot, J, which for the case of proportionate coupling to the leads, $\Gamma^{L}_{\sigma}(\omega)=\alpha\Gamma^{R}_{\sigma}(\omega)$, can be expressed[3,4,22] in terms of the density of states $\rho_{\sigma}(\omega)$ as

$$J=\frac{e}{\hbar}\sum_{\sigma}\int_{-\infty}^{\infty}d\omega[f_L(\omega)-f_R(\omega)]\Gamma_{\sigma}(\omega)\rho_{\sigma}(\omega)\,, \tag{3}$$

where $\Gamma_{\sigma}(\omega)=\Gamma^{L}_{\sigma}(\omega)\Gamma^{R}_{\sigma}(\omega)/[\Gamma^{L}_{\sigma}(\omega)+\Gamma^{R}_{\sigma}(\omega)]$. The density of states is given by

$$\rho_{\sigma}(\omega)=-\frac{1}{\pi}\,\mathrm{Im}G^{r}_{\sigma}(\omega)\,, \tag{4}$$

where $G^{r}_{\sigma}(\omega)$ is the Fourier transform of the retarded Green function,

$$G^{r}_{\sigma}(t)=-i\theta(t)\langle\{c_{\sigma}(t),c^{\dagger}_{\sigma}(0)\}\rangle\,. \tag{5}$$

2. The slave-boson Hamiltonian

Diagrammatic techniques are reliable when the expansion parameter is a small quantity. For an Anderson impurity with $U\to\infty$, it is natural to perturb in the hopping strength. However, the standard diagrammatic approach also requires that the unperturbed Hamiltonian be noninteracting, i.e., quadratic in the second-quantized operators. In the limit of infinite U, the bare Hamiltonian can be made quadratic by transforming the Hamiltonian (1) into a new Hamiltonian, expressed in terms of new local operators.[23,24] These operators create the three pos-

sible states of the site: a boson operator $\mathbf{b}^\dagger$, which creates an empty site, and two fermion operators, $\mathbf{f}_\sigma^\dagger$, which create the singly occupied states. The ordinary electron operators on the site, which transform the empty site into a singly occupied site or vice versa, are decomposed into a boson operator and a fermion operator,

$$\begin{aligned}\mathbf{c}_\sigma(t)&=\mathbf{b}^\dagger(t)\mathbf{f}_\sigma(t)\ ,\\ \mathbf{c}_\sigma^\dagger(t)&=\mathbf{f}_\sigma^\dagger(t)\mathbf{b}(t)\ .\end{aligned}\tag{6}$$

The slave boson in (6) acts as a bookkeeping device which prevents double occupancy of the site: when an electron creation operator acts on an occupied site, the boson part acting on the vacuum annihilates the state, $\mathbf{c}_\sigma^\dagger\mathbf{f}_{\bar\sigma}^\dagger|\Omega\rangle=\mathbf{f}_\sigma^\dagger\mathbf{b}\mathbf{f}_{\bar\sigma}^\dagger|\Omega\rangle=0$. (In these expressions $|\Omega\rangle$ is the vacuum state.)

In the slave boson representation, the Hamiltonian for the infinite-U Anderson model becomes

$$\begin{aligned}H=&\sum_{\sigma;k\in L,R}\epsilon_{k\sigma}\mathbf{c}_{k\sigma}^\dagger\mathbf{c}_{k\sigma}+\sum_\sigma\epsilon_\sigma\mathbf{f}_\sigma^\dagger\mathbf{f}_\sigma\\&+\sum_{\sigma;k\in L,R}(V_{k\sigma}\mathbf{c}_{k\sigma}^\dagger\mathbf{b}^\dagger\mathbf{f}_\sigma+\text{H.c.})\ .\end{aligned}\tag{7}$$

The first two terms form the unperturbed, quadratic Hamiltonian and the last term, which represents hopping between site and leads, can be handled as a perturbation. The fermions and boson are treated as ordinary particles in the perturbation expansion. For example, the lowest-order diagrams are shown for the boson and fermion propagators in Fig. 2. While summation of a few low-order diagrams is possible,[23,25] techniques are also available to sum whole classes of diagrams. In the end, whatever approach is taken, properties of the physical electrons can be constructed from the results for the boson and fermions.

There is, however, an added constraint, as the site can only be in one of the states $\mathbf{b}^\dagger|\Omega\rangle$ and $\mathbf{f}_\sigma^\dagger|\Omega\rangle$. Accordingly, in all physical states, the number of bosons plus the number of fermions,

$$Q=\mathbf{b}^\dagger\mathbf{b}+\sum_\sigma\mathbf{f}_\sigma^\dagger\mathbf{f}_\sigma\ ,\tag{8}$$

must be equal to unity. We will show below, when we describe the Keldysh diagrammatic approach, how this constraint is dealt with.

(a) boson propagator

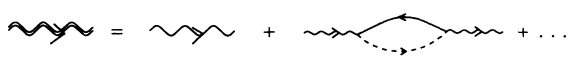

(b) fermion propagator

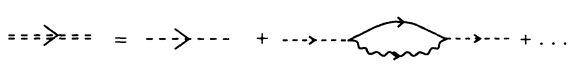

FIG. 2. Diagrammatic expansion for (a) the slave-boson and (b) the fermion propagators. The coupling between site and leads is treated as the perturbation, so each vertex corresponds to a tunneling event.

3. *The Keldysh formalism*

Previous diagrammatic calculations using the slave-boson representation[20] have addressed equilibrium properties of the Anderson model. Since our focus is on nonequilibrium properties a different approach is required. Specifically, we employ the Keldysh[26,27] rather than the Matsubara[28] formalism. The main complication with nonequilibrium is that the basis of the equilibrium diagrammatic approach, the fact that the state of the system at $t=+\infty$ is identical to the state of the system at $t=-\infty$, up to a phase (Gell-Mann and Low theorem[29]), is no longer valid. Since in a nonequilibrium system real dissipation can occur, the state of the system is in general not known at $t=+\infty$ and one must relate all quantities to the state of the system at $t=-\infty$. In practice, this means that instead of having integrals from $t=-\infty$ to $t=+\infty$ as in the usual zero-temperature formulation,[30] all integrals have to be carried out along a path that starts and ends at $t=-\infty$ (Fig. 3). Consequently, a Green function will depend not only on the times at which the operators act, but also on the corresponding branch of the contour. Thus the Green functions carry additional indices, and the usual perturbation expansion, or the Dyson equation, takes a matrix form. In all, there are three independent types of two-particle Green functions in nonequilibrium. It is convenient to choose, in addition to the retarded Green function (5), the two Green functions:

$$\begin{aligned}G_\sigma^<(t)&=i\langle\mathbf{c}_\sigma^\dagger(0)\mathbf{c}_\sigma(t)\rangle\ ,\\ G_\sigma^>(t)&=-i\langle\mathbf{c}_\sigma(t)\mathbf{c}_\sigma^\dagger(0)\rangle\ ,\end{aligned}\tag{9}$$

as they carry information on the occupation of the site.

For the problem at hand, at the starting point at $t=-\infty$ the Anderson impurity and the leads are unconnected and separately at equilibrium, possibly with different chemical potentials. Formally, the hopping is turned on slowly, and nonequilibrium properties are evaluated long after the hopping is fully established, when a steady state has been achieved, but before current flow has changed the chemical potentials deep in the leads.

Before applying the Keldysh formalism to the slave-boson Hamiltonian (7), one has to overcome the difficulty associated with the constraint that the physical states are restricted to the $Q=1$ ensemble. Specifically, it is not

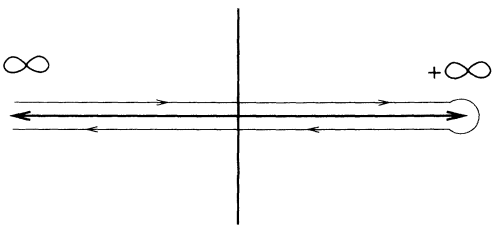

FIG. 3. Real-time contour for nonequilibrium Green functions in the Keldysh formalism.

convenient to perform diagrammatic calculations (Keldysh or Matsubara) in a restricted ensemble since Dyson's equation does not apply. Instead, we introduce a complex chemical potential,[20] calculate diagrams in an unrestricted ensemble treating the hopping as a perturbation, and finally use the complex chemical potential to project to the $Q=1$ subspace. In practice, this projection corresponds to keeping only an easily identified subset of diagrams.

To formulate the Keldysh diagrammatic theory in terms of a complex chemical potential, it is convenient to start with a formal expression for expectation values in nonequilibrium. In the $Q=1$ ensemble, the expectation value of an operator $\mathbf{O}$ can be written as

$$\langle \mathbf{O} \rangle_{Q=1} = \frac{1}{Z_{Q=1}} \mathrm{Tr}\{ e^{-\beta(H_0-\mu_L N_L-\mu_R N_R)} \times \delta_{Q,1} T_C[S_C(-\infty,-\infty)\mathbf{O}]\} , \quad (10)$$

where T_C orders operators along the Keldysh contour (Fig. 3) and the partition function is given by

$$Z_{Q=n} = \mathrm{Tr}\{ e^{-\beta(H_0-\mu_L N_L-\mu_R N_R)} \times \delta_{Q,n} T_C[S_C(-\infty,-\infty)]\} , \quad (11)$$

with $Q=1$. In (10), the system evolves under the action of the Hamiltonian so that

$$S_C(-\infty,-\infty) = \exp\left[-i \oint_C dt' H(t') \right] . \quad (12)$$

Importantly, the operator $\mathbf{O}$ may include parts acting at different times, e.g., $\mathbf{O}=i\mathbf{c}_\sigma^\dagger(0)\mathbf{c}_\sigma(t)$ would give the nonequilibrium expectation value of the "lesser" Green function $G_\sigma^<(t)$. Since the Hamiltonian commutes with the sum of bosons and fermions Q the projection to the $Q=1$ ensemble is accomplished once and for all by the factor $\delta_{Q,1}$ in (10). It is not necessary to include a chemical potential for the impurity since local expectation values in the coupled system are independent of the initial state of the impurity.

To transform to an ensemble where Q is unconstrained,[20] one rewrites the Kronecker δ as an integral over a complex chemical potential $i\lambda$,

$$\delta_{Q,1} = \frac{\beta}{2\pi} \int_{-\pi/\beta}^{\pi/\beta} d\lambda \, e^{-i\beta\lambda(Q-1)} . \quad (13)$$

Dividing both numerator and denominator of (10) by $Z_{Q=0}$ gives[31]

$$\langle \mathbf{O} \rangle_{Q=1} = \frac{Z_{Q=0}}{Z_{Q=1}} \frac{\beta}{2\pi} \int_{-\pi/\beta}^{\pi/\beta} d\lambda \, e^{i\beta\lambda} \langle \mathbf{O} \rangle_{i\lambda} = \frac{Z_{Q=0}}{Z_{Q=1}} \langle \mathbf{O} \rangle_{i\lambda}^{(1)} , \quad (14)$$

where

$$\langle \mathbf{O} \rangle_{i\lambda} = \frac{1}{Z_{i\lambda}} \mathrm{Tr}\{ e^{-\beta(H_0-\mu_L N_L-\mu_R N_R+i\lambda Q)} \times T_C[S_C(-\infty,-\infty)\mathbf{O}]\} . \quad (15)$$

In (14), $\langle \mathbf{O} \rangle_{i\lambda}^{(1)}$ is the coefficient of the term of order $\exp(-i\beta\lambda)$ in $\langle \mathbf{O} \rangle_{i\lambda}$. The important point is that $\langle \mathbf{O} \rangle_{i\lambda}$ in (15) is in the standard form for diagrammatic perturbation theory since the trace in (15) and in the partition function

$$Z_{i\lambda} = \mathrm{Tr}\{ e^{-\beta(H_0-\mu_L N_L-\mu_R N_R+i\lambda Q)} T_C[S_C(-\infty,-\infty)]\} \quad (16)$$

are taken over all states without restriction to $Q=1$.

According to (14), the nonequilibrium expectation value of an operator $\mathbf{O}$ in the $Q=1$ ensemble has two contributions: a normalization factor $Z_{Q=0}/Z_{Q=1}$, and the coefficient of $\exp(-i\beta\lambda)$ for the same operator in the $i\lambda$ ensemble. The normalization can be obtained from the identity $\langle Q \rangle_{Q=1}=1$, which implies

$$\frac{Z_{Q=1}}{Z_{Q=0}} = \langle \mathbf{b}^\dagger \mathbf{b} \rangle_{i\lambda}^{(1)} + \sum_\sigma \langle \mathbf{f}_\sigma^\dagger \mathbf{f}_\sigma \rangle_{i\lambda}^{(1)} . \quad (17)$$

The expectation value $\langle \mathbf{O} \rangle_{i\lambda}^{(1)}$, as well as the expectation values appearing on the right-hand side of Eq. (17), can be obtained diagrammatically.

B. Noncrossing approximation

To obtain a well-behaved density of states from the nonequilibrium perturbation theory, one needs some way of summing diagrams to all orders in the hopping. In finite-order perturbation theory there are divergences associated with the bare levels ϵ_σ and, at $T=0$, logarithmic divergences near the chemical potentials due to the Kondo effect.[25] To control these divergences, we employ the noncrossing approximation, which has been used successfully to treat the infinite-U Anderson model in equilibrium.[20] As can be seen from Fig. 2, at lowest order in perturbation theory the boson self-energy involves the fermion propagator while the fermion self-energy involves the boson propagator. By using the two relations self-consistently—the noncrossing approximation, see Fig. 4—one obtains a set of coupled integral equations, which can be solved numerically. Solving these self-consistent equations corresponds to summing a subset of diagrams to all orders in the hopping matrix element V. It can be shown[20] that all diagrams of leading order in $1/N$, where N is the number of spin degrees of freedom, are included

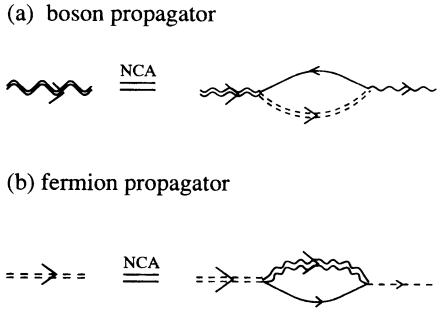

FIG. 4. Diagrammatic representation of the noncrossing approximation. (a) Dyson's equation for the boson propagator includes the fermion propagators in the self-energy, and (b) Dyson's equation for each fermion propagator includes the boson propagator in the self-energy.

in this subset. Therefore, the noncrossing approximation is expected to be a quantitative approach in the limit of large N. For the case, $N=2$, of interest for quantum dots, Cox[32] has shown that the calculated equilibrium occupancy and susceptibility agree with the exact Bethe-ansatz results to within the 0.5% convergence accuracy of the noncrossing approximation. (As we will discuss in Sec. II D, the noncrossing approximation is less accurate for the conductance due to an overestimate of the Kondo peak amplitude. At worst, the linear-response conductance is overestimated by 15%, and this can be taken as a limit on the quantitative accuracy of our results.) Here, we generalize the noncrossing approximation to nonequilibrium. The equations will involve not only the retarded Green function, but also the lesser and greater ones, leading to slightly more complicated equations than at equilibrium.

Since our goal is to calculate the nonequilibrium current, we will calculate first the density of states for the Anderson impurity, $\rho_\sigma(\omega)$, and obtain the current from Eq. (3). To find the density of states for $U\to\infty$, we need the retarded Green function (4) in the ensemble with complex chemical potential (14),

$$\rho_\sigma(\omega)=\frac{Z_{Q=0}}{Z_{Q=1}}\left[-\frac{1}{\pi}\,\mathrm{Im}G^{r(1)}_{\sigma,i\lambda}(\omega)\right] . \tag{18}$$

Within the noncrossing approximation, the retarded Green function is expressed in terms of the full propagators for boson and fermion as

$$\begin{aligned} G^{r(1)}_{\sigma,i\lambda}(t)&\equiv -i\theta(t)\langle\{\mathbf{c}_\sigma(t),\mathbf{c}^\dagger_\sigma(0)\}\rangle^{(1)}_{i\lambda} \\ &\overset{\text{NCA}}{=} -i\theta(t)[D^{>}(-t)G^{<}_{f\sigma}(t) \\ &\qquad -D^{<}(-t)G^{>}_{f\sigma}(t)] , \end{aligned} \tag{19}$$

where

$$\begin{aligned} D^{>}(t)&\equiv -i\langle\mathbf{b}(t)\mathbf{b}^\dagger(0)\rangle^{(0)}_{i\lambda} , \\ D^{<}(t)&\equiv -i\langle\mathbf{b}^\dagger(0)\mathbf{b}(t)\rangle^{(1)}_{i\lambda} , \\ G^{>}_{f\sigma}(t)&\equiv -i\langle\mathbf{f}_\sigma(t)\mathbf{f}^\dagger_\sigma(0)\rangle^{(0)}_{i\lambda} , \\ G^{<}_{f\sigma}(t)&\equiv i\langle\mathbf{f}^\dagger_\sigma(0)\mathbf{f}_\sigma(t)\rangle^{(1)}_{i\lambda} . \end{aligned} \tag{20}$$

Equation (19) is straightforward to obtain by decomposing the electron operators into boson and fermion operators (6) and then factorizing the boson and fermion parts. The latter step corresponds to a neglect of vertex corrections. Since each term in (19) contains exactly one lesser operator, with a boson or fermion lowering operator acting directly to the right, the overall result is $O[\exp(-i\beta\lambda)]$ as required.

Because the Hamiltonian is time independent, it is simplest to evaluate the boson and fermion Green functions in the frequency representation. The physical density of states is then given by

$$\begin{aligned} \rho_\sigma(\omega)=\frac{1}{4\pi^2}\frac{Z_{Q=0}}{Z_{Q=1}}\int_{-\infty}^{\infty}d\omega'[&D^{>}(\omega')G^{<}_{f\sigma}(\omega+\omega') \\ &-D^{<}(\omega')G^{>}_{f\sigma}(\omega+\omega')] . \end{aligned} \tag{21}$$

The noncrossing approximation is represented diagrammatically in Fig. 4: the boson and fermion propagators are each assigned a single self-energy bubble (albeit determined self-consistently) and the self-energies are iterated to all orders via Dyson's equation. Standard manipulation of the nonequilibrium Dyson equations then leads to[33]

$$\begin{aligned} D^{\lessgtr}(\omega)&=D^{r}(\omega)\Pi^{\lessgtr}(\omega)D^{a}(\omega) , \\ G^{\lessgtr}_{f\sigma}(\omega)&=G^{r}_{f\sigma}(\omega)\Sigma^{\lessgtr}_{f\sigma}(\omega)G^{a}_{f\sigma}(\omega) , \end{aligned} \tag{22}$$

where the self-energies are given by

$$\begin{aligned} \Pi^{\lessgtr}(\omega)&=-\frac{i}{2\pi}\int_{-\infty}^{\infty}d\omega'\sum_{\sigma;k\in L,R}|V_{k\sigma}|^2g^{\gtrless}_{k\sigma}(\omega'-\omega) \\ &\qquad\times G^{\lessgtr}_{f\sigma}(\omega') , \\ \Sigma^{\lessgtr}_{f\sigma}(\omega)&=\frac{i}{2\pi}\int_{-\infty}^{\infty}d\omega'\sum_{k\in L,R}|V_{k\sigma}|^2g^{\lessgtr}_{k\sigma}(\omega-\omega')D^{\lessgtr}(\omega') . \end{aligned} \tag{23}$$

In (23), the lower-case g's are the Green functions of electrons in the leads not coupled to the site,[34]

$$\begin{aligned} g^{>}_{k\sigma}(\omega)&=-2\pi i[1-f_{L(R)}(\omega)]\delta(\omega-\epsilon_{k\sigma}) , \\ g^{<}_{k\sigma}(\omega)&=2\pi i f_{L(R)}(\omega)\delta(\omega-\epsilon_{k\sigma}) . \end{aligned} \tag{24}$$

Several other relations are required to close the equations for the noncrossing approximation. The retarded Green functions for the boson and fermions in (22) are given by[33]

$$\begin{aligned} D^{r}(\omega)&=\frac{1}{\omega-\Pi^{r}(\omega)} , \\ G^{r}_{f\sigma}(\omega)&=\frac{1}{\omega-\epsilon_\sigma-\Sigma^{r}_{f\sigma}(\omega)} , \end{aligned} \tag{25}$$

where the retarded self-energies are Hilbert transforms of the greater self-energies

$$\begin{aligned} \Pi^{r}(\omega)&=\frac{i}{2\pi}\int_{-\infty}^{\infty}d\omega'\frac{\Pi^{>}(\omega')}{\omega-\omega'+i\eta} , \\ \Sigma^{r}_{f\sigma}(\omega)&=\frac{i}{2\pi}\int_{-\infty}^{\infty}d\omega'\frac{\Sigma^{>}_{f\sigma}(\omega')}{\omega-\omega'+i\eta} . \end{aligned} \tag{26}$$

The advanced Green functions D^a and $G^a_{f\sigma}$ in (22) are complex conjugates of the retarded Green functions D^r and $G^r_{f\sigma}$. Equations (26) follow because, by definition, all retarded Green functions and self-energies can be written as a difference of greater and lesser functions, $G^r(t)=\theta(t)[G^{>}(t)-G^{<}(t)]$. In the $i\lambda$ ensemble, the lesser functions for the boson and fermions are $O[\exp(-i\beta\lambda)]$ and must be dropped from the retarded functions which are $O(1)$. One therefore has the useful relations:

$$\begin{aligned} D^{>}(\omega)&=2i\,\mathrm{Im}D^{r}(\omega) , \\ G^{>}_{f\sigma}(\omega)&=2i\,\mathrm{Im}G^{r}_{f\sigma}(\omega) , \end{aligned} \tag{27}$$

for the boson and fermion Green functions, and

$$\begin{aligned} \Pi^{>}(\omega)&=2i\,\mathrm{Im}\Pi^{r}(\omega) , \\ \Sigma^{>}_{f\sigma}(\omega)&=2i\,\mathrm{Im}\Sigma^{r}_{f\sigma}(\omega) , \end{aligned} \tag{28}$$

for the self-energies.

The closed set of equations for the noncrossing approximation can be solved iteratively. In practice, we start with an initial guess for the greater boson Green function $D^{>}(\omega)$, calculate $\Sigma^{r}_{f\sigma}(\omega)$ for each spin by combining (23) and (26), and use (25) to get $G^{r}_{f\sigma}(\omega)$. The values for the greater fermion Green functions, from $G^{>}_{f\sigma}(\omega) = 2i\,\mathrm{Im}G^{r}_{f\sigma}(\omega)$, can then be used in a parallel way to obtain an improved $D^{>}(\omega)$. This procedure is iterated to convergence. A similar procedure is then followed for the lesser Green functions. Following an initial guess for $D^{<}(\omega)$, the fermion self-energies $\Sigma^{<}_{f\sigma}(\omega)$ are obtained from (23), and $G^{<}_{f\sigma}(\omega)$ is determined from (22). The steps are repeated for $D^{<}(\omega)$, and the process iterated to convergence. Finally, the physical density of states $\rho_{\sigma}(\omega)$ is evaluated by the convolution of the boson and fermion Green functions in (21).

C. Numerical methods

In this section, we describe in greater detail the numerical procedures we have used to solve the nonequilibrium, self-consistent equations for the noncrossing approximation. Following the equilibrium work,[20,32] we take the energy dependence of the coupling between the site and the leads (2) to be Lorentzian

$$\Gamma^{L(R)}_{\sigma}(\omega) = 2\pi \sum_{k\in L(R)} |V_{k\sigma}|^2 \delta(\omega-\epsilon_{k\sigma}) \equiv \Gamma^{L(R)}_{0\sigma} \frac{W^2}{(\omega-\epsilon_{L(R)})^2+W^2} . \tag{29}$$

The finite width W reflects the finite bandwidth in the leads and is necessary to prevent ultraviolet divergence of the results.[35] In principle, the bands in the leads can be centered at different energies, but the validity of Eq. (3) for the current requires $\Gamma^{L}_{\sigma}(\omega) = \alpha\Gamma^{R}_{\sigma}(\omega)$, so we take $\epsilon_L = \epsilon_R = \epsilon_0 = 0$, throughout. [An expression (A1) for the current in the absence of this condition is given in the Appendix.] The choice of a Lorentzian form allows a simplification of the self-consistent equations.[36] In general, to iterate the noncrossing approximation equations, the retarded self-energies for the boson and fermions (26) must be evaluated by double integrals over the greater Green function of the other species. For the Lorentzian coupling, however, one of these integrals can be performed analytically. First, combining Eqs. (23) and (26), the boson retarded self-energy can be written as a single integral,

$$\Pi^{r}(\omega) = \sum_{\sigma}\sum_{L,R} \int_{-\infty}^{\infty} d\omega' H^{L(R)}_{\sigma}(\omega'-\omega) G^{>}_{f\sigma}(\omega') , \tag{30}$$

with the kernels

$$H^{L(R)}_{\sigma}(\omega) = \frac{1}{(2\pi)^2}\Gamma^{L(R)}_{\sigma}(\omega)\left[\pi f_{L(R)}(\omega) + i\,\mathrm{Re}\left[\Psi\left[\frac{1}{2}-\frac{i\beta(\omega-\mu_{L(R)})}{2\pi}\right]-\Psi\left[\frac{1}{2}+\frac{\beta[W-i(\epsilon_{L(R)}-\mu_{L(R)})]}{2\pi}\right]\right]\right.$$
$$\left. -i\frac{\omega-\epsilon_{L(R)}}{W}\left\{\frac{\pi}{2}+\mathrm{Im}\left[\Psi\left[\frac{1}{2}+\frac{\beta[W-i(\epsilon_{L(R)}-\mu_{L(R)})]}{2\pi}\right]\right]\right\}\right] . \tag{31}$$

In (31), β is the inverse temperature and $\Psi(z)$ is the Digamma function.[37] Second, the fermion retarded self-energies can be written as single integrals

$$\Sigma^{r}_{f\sigma}(\omega) = \sum_{L,R} \int_{-\infty}^{\infty} d\omega' K^{L(R)}_{\sigma}(\omega-\omega') D^{>}(\omega') , \tag{32}$$

with the kernels

$$K^{L(R)}_{\sigma}(\omega) = \frac{1}{(2\pi)^2}\Gamma^{L(R)}_{\sigma}(\omega)\left[\pi[1-f_{L(R)}(\omega)] + i\,\mathrm{Re}\left[\Psi\left[\frac{1}{2}-\frac{i\beta(\omega-\mu_{L(R)})}{2\pi}\right]-\Psi\left[\frac{1}{2}+\frac{\beta[W-i(\epsilon_{L(R)}-\mu_{L(R)})]}{2\pi}\right]\right]\right.$$
$$\left. +i\frac{\omega-\epsilon_{L(R)}}{W}\left\{\frac{\pi}{2}-\mathrm{Im}\left[\Psi\left[\frac{1}{2}+\frac{\beta[W-i(\epsilon_{L(R)}-\mu_{L(R)})]}{2\pi}\right]\right]\right\}\right] . \tag{33}$$

Since the greater Green functions and self-energies are just the imaginary parts of the corresponding retarded functions (27) and (28), the above equations, together with the relation (25) between the retarded Green functions and self-energies, form a closed set. In practice, we make an initial guess for the greater boson Green function and then iterate the equations to convergence. Typically the results converge within five iterations. We have checked the accuracy of the results by comparing to the sum rules on the boson and fermion Green functions

$$\int_{-\infty}^{\infty} d\omega \left[-\frac{1}{\pi}\mathrm{Im}D^{r}(\omega)\right] = 1 ,$$
$$\int_{-\infty}^{\infty} d\omega \left[-\frac{1}{\pi}\mathrm{Im}G^{r}_{f\sigma}(\omega)\right] = 1 . \tag{34}$$

These relations are always satisfied to better than 0.5% by the converged numerical solutions.

A separate iterative loop is required to evaluate the

lesser Green functions and self-energies. Equations (23) for the boson and fermion lesser self-energies can be rewritten as

$$\Pi^{<}(\omega)=-\frac{1}{2\pi}\sum_{\sigma}\sum_{L,R}\int_{-\infty}^{\infty}d\omega'\Gamma_{\sigma}^{L(R)}(\omega'-\omega)\times[1-f_{L(R)}(\omega'-\omega)]G_{f\sigma}^{<}(\omega') \tag{35}$$

and

$$\Sigma_{f\sigma}^{<}(\omega)=-\frac{1}{2\pi}\sum_{L,R}\int_{-\infty}^{\infty}d\omega'\Gamma_{\sigma}^{L(R)}(\omega-\omega')\times f_{L(R)}(\omega-\omega')D^{<}(\omega') . \tag{36}$$

Together with Eqs. (22), these form a closed set of equations for the lesser Green functions and self-energies. Again, following an initial guess for the boson lesser Green function, these equations are iterated to convergence. Since the lesser Green functions have an arbitrary overall normalization, to check the convergence it is necessary to monitor a normalized quantity. We choose, for simplicity, to monitor the occupation of each spin state

$$\langle n_{\sigma}\rangle=\frac{Z_{Q=0}}{Z_{Q=1}}\left[-\frac{i}{2\pi}\int_{-\infty}^{\infty}d\omega\, G_{f\sigma}^{<}(\omega)\right] , \tag{37}$$

where the normalization is provided by the ratio of partition functions, which from Eq. (17) is given by

$$\frac{Z_{Q=1}}{Z_{Q=0}}=\frac{i}{2\pi}\int_{-\infty}^{\infty}d\omega\left[D^{<}(\omega)-\sum_{\sigma}G_{f\sigma}^{<}(\omega)\right] . \tag{38}$$

Typically, within five iterations the occupations converge to better than 0.01%. However, one cannot expect the accuracy of the results to be better than the accuracy of 0.5% found for the retarded Green functions, from which the lesser functions are constructed via (22). The final accuracy is verified by the sum rule for infinite U relating the total density of states of one spin state to the occupancy of all the other spin states

$$\int_{-\infty}^{\infty}d\omega\,\rho_{\sigma}(\omega)=1-\sum_{\sigma'\neq\sigma}\langle n_{\sigma'}\rangle . \tag{39}$$

This relation is always satisfied to within 0.5%.

The procedure has also been checked by comparing to the equilibrium results,[36] and excellent agreement is found. This is an independent check since much of our numerical procedure differs from that used in equilibrium. Importantly, because there are multiple sharp features in the nonequilibrium density of states (discussed in the following section), we have used a self-adjusting mesh for the numerical integrations rather than the logarithmic mesh used in the equilibrium case.[20,32] We have also found that evaluating the Green functions on the range $[-10W,10W]$ is sufficient for numerical accuracy. The wider range used previously[20,32] is unnecessary because the kernels (31) and (33) contain all the effects of the long band tails in the leads.

D. Results of the noncrossing approximation

In this section, we present numerical results of the noncrossing approximation for an Anderson impurity in and out of equilibrium.

1. *Linear-response conductance*

The equilibrium properties, calculated by the noncrossing approximation, can be used to predict quantitatively the line shape of the linear-response conductance peak. To our knowledge, this is the first detailed prediction of the conductance peak evolution in the Kondo regime. From Eq. (3) the linear-response conductance is given by

$$\sigma=2\pi\frac{e^2}{h}\sum_{\sigma}\int_{-\infty}^{\infty}d\omega[-f'(w)]\Gamma_{\sigma}(\omega)\rho_{\sigma}(\omega) , \tag{40}$$

where $\rho_{\sigma}(\omega)$ is calculated at equilibrium, and $f'(w)$ is the derivative of the equilibrium Fermi function. In Fig. 5 we plot the equilibrium density of states (21) of an Anderson impurity with two degenerate spin states, for one value of chemical potential ($\mu-\epsilon_0=2\Gamma$). There is a sharp Kondo peak at the chemical potential. Its amplitude increases with decreasing temperature down to the Kondo temperature,[20] $T_K\simeq W(\Gamma/2\pi(\mu-\epsilon_0))^{1/2}\exp[-\pi(\mu-\epsilon_0)/\Gamma]$, where it saturates. In

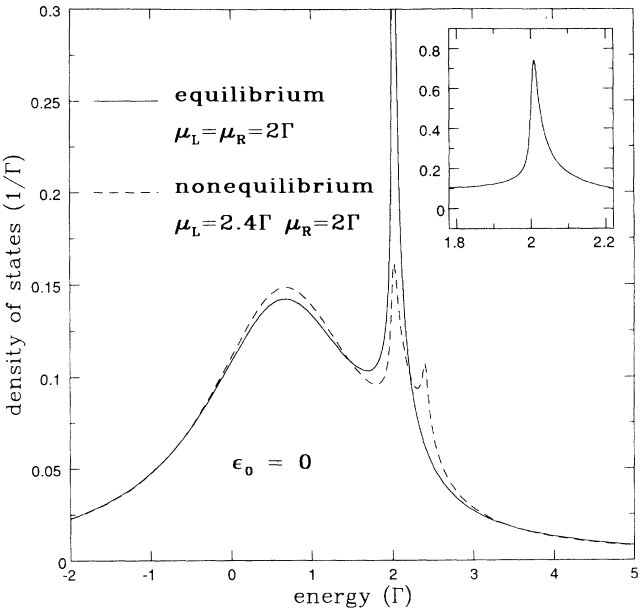

FIG. 5. Equilibrium and nonequilibrium density of states $\rho_{\sigma}(\omega)$ for an Anderson impurity symmetrically coupled to two leads of Lorentzian bandwidth $2W$ and chemical potentials μ_L and μ_R. The impurity has two degenerate spin states at energy $\epsilon_0=0$, and an on-site interaction $U\to\infty$. With all energies in units of the total coupling to the leads Γ, the band half width at half maximum is $W=100$ and the temperature is $T=0.005$. At equilibrium (solid curve) there is a single Kondo peak in the density of states at the chemical potential $\mu_L=\mu_R=2$ (see inset). Out of equilibrium (dashed curve), the peak splits into two suppressed peaks, one at each chemical potential, $\mu_L=2.4$ and $\mu_R=2$.

Fig. 6(a), the resulting linear-response conductance obtained from (40) is plotted as the chemical potential is swept through the bare-level energy at three different temperatures. Several features are noteworthy. First, as the temperature is initially lowered, the width of the conductance peak decreases proportionally to $k_B T$, because the peak line shape is determined by the derivative of the Fermi function (40). As the temperature is lowered below Γ, the peak width is expected to be dominated by Γ and to saturate. Here, however, for $k_B T \lesssim 0.075\Gamma$, the conductance peak begins to broaden again. This broadening is entirely due to the appearance of the Kondo peak in the density of states, and is therefore a signature of the Kondo effect. Second, as temperature is lowered, the peak amplitude increases and finally saturates. The saturated open-channel conductance $\sigma = 2e^2/h$ is only achieved for a dot symmetrically coupling to its leads; otherwise, the conductance is reduced by the asymmetry factor $4\Gamma_{0\sigma}^L \Gamma_{0\sigma}^R / (\Gamma_{0\sigma}^L + \Gamma_{0\sigma}^R)$. Third, the peak maximum shifts to higher chemical potential[19] and the tails become power law (roughly Lorentzian) rather than exponential as at higher temperatures. It is interesting to note that the conductance peak remains nearly symmetric with decreasing temperature despite the very asymmetric behavior of the density of states, which has a Kondo peak only for $\mu > \epsilon_0$. For comparison, the total occupancy of the site is plotted as a function of chemical potential in Fig. 6(b). Unlike the conductance, the total occupancy is not sensitive to the behavior near the Fermi surface, and therefore does not show any obvious signature of the Kondo effect.

The temperature dependences of the main features of the conductance peak are plotted in Fig. 7. Over a broad range of temperatures the peak width, amplitude, and position increase roughly logarithmically with temperature. This reflects the logarithmic scaling of interactions which is the well-known signature of the Kondo effect in perturbation theory.[38] For $k_B T \lesssim 0.005\Gamma$, the peak amplitude saturates while the peak position and width continue to increase.

The results for the equilibrium conductance obtained from the noncrossing approximation are almost entirely consistent with the predictions of Glazman and Raikh[17] and Ng and Lee.[18] The primary prediction that the conductance peak should broaden and increase in amplitude to $\sigma = 2e^2/h$ with decreasing temperature is certainly borne out. The broadening is also observed to occur only on the high-chemical-potential side, where the Kondo effect enhances the conductance. However, the speculation by Ng and Lee that this one-sided broadening would lead to a noticeably asymmetric peak shape is not supported by our results down to $k_B T = 0.005\Gamma$. The roughly logarithmic one-sided broadening of the peak is compensated by a logarithmic shift of the peak maximum. The final result is a nearly symmetric peak centered at a higher chemical potential. At lower temperatures the peak may still become asymmetric, but the numerical convergence of the noncrossing approximation becomes unreliable in this regime.

Note that the noncrossing approximation is known to overestimate the Kondo peak amplitude somewhat for chemical potentials within a few Γ of the bare-level energies.[39] The true magnitude of the conductance peak for a

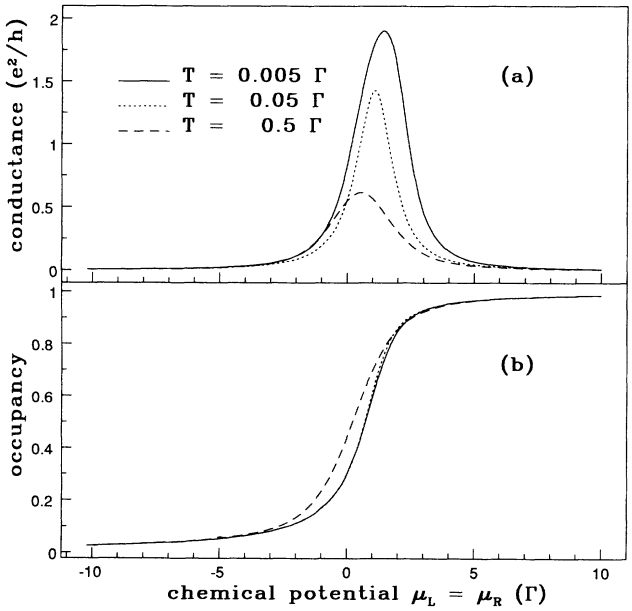

FIG. 6. (a) Linear-response conductance σ through an Anderson impurity for three different temperatures as a function of chemical potential. The impurity has two degenerate spin states at $\epsilon_0 = 0$. The conductance peak first narrows and then broadens with decreasing temperature. (b) Total site occupancy $n_\uparrow + n_\downarrow$ as a function of chemical potential for the same temperatures.

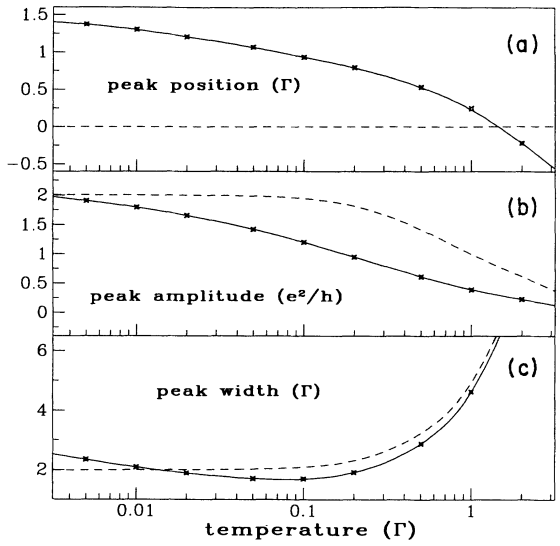

FIG. 7. (a) Temperature dependence of the linear-response conductance peak position. (b) Temperature dependence of the conductance peak amplitude. (c) Temperature dependence of the conductance peak full width at half maximum. In all three panels, the noncrossing approximation results are the data points and the solid curve is a guide to the eye. For comparison, the dashed curves are the exact results for noninteracting levels.

symmetric structure is therefore not expected to approach the maximum value, $2e^2/h$, until temperatures below those shown in Fig. 6. For example, taking the saturated low-temperature value for $\langle n_\sigma \rangle$ from Fig. 6(b), which is known to be reliable,[32] and using Langreth's exact relation for zero temperature[40]

$$\sigma = 2\frac{e^2}{h}\sin^2(\pi\langle n_\sigma \rangle) , \tag{41}$$

one obtains a conductance $\sigma = 1.63e^2/h$ at the peak of the lowest temperature curve in Fig. 6(a). The observed peak value of $\sigma = 1.90e^2/h$ is therefore 15% higher than the expected zero-temperature value, and must be an overestimate. However, at higher chemical potentials $\langle n_\sigma \rangle \to \frac{1}{2}$, so the exact result for the conductance approaches $\sigma = 2e^2/h$ at zero temperature. In this regime, the noncrossing approximation faithfully reproduces the exact result.[39]

2. *Nonequilibrium*

There are qualitatively new features in the nonequilibrium density of states compared to equilibrium. In Fig. 5, the density of states (21) of an Anderson impurity with two degenerate spin states is plotted both for equilibrium and for nonequilibrium, where the two leads have different chemical potentials. There are striking differences between equilibrium (solid curve) and nonequilibrium (dashed curve). In equilibrium there is a single Kondo peak at the chemical potential. Out of equilibrium, the Kondo peak splits into two smaller peaks, one at each chemical potential. With decreasing temperature, the amplitudes of these peak *do not* increase to the unitarity limit, but saturate at a much lower value. This saturation occurs at a temperature above T_K, and results from dissipative processes in which an electron is transferred from the lead with higher chemical potential to the lead with lower chemical potential. The noncrossing approximation specifically includes these processes since it has contributions from all orders in the hopping. However, from the numerical results of the noncrossing approximation it is difficult to extract the magnitude of this dissipative lifetime. Instead, in the next section, we present an analytical estimate of the dissipative lifetime obtained via a perturbative approach.

A clear signature of the Kondo effect is expected in the nonlinear current. For chemical potentials above the bare-level energy, the linear-response conductance is dominated by the narrow Kondo peak in the density of states. In nonlinear response, at low temperatures, the current J is determined by an integral of the density of states between the two chemical potentials (3). Therefore, as soon as the chemical-potential difference exceeds the width of the Kondo peak, the differential conductance will fall off dramatically. Moreover, the Kondo peak will split and the split peaks decrease in amplitude with increasing chemical potential (Fig. 5). The net effect is a sharp maximum peak in the differential conductance around zero bias, for $\mu > \epsilon_0$.[3,4] In Fig. 8, we have plotted the differential conductance as a function of chemical-potential difference, or equivalently voltage bias, at two

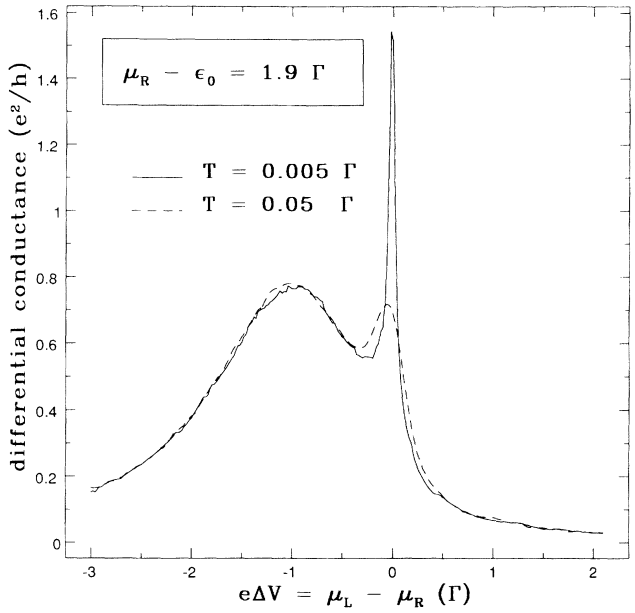

FIG. 8. Differential conductance $e\,dJ/d\Delta\mu$, with $\mu_R = 1.9$ vs applied bias, at two temperatures, $k_BT = 0.005$ and 0.05. The peak in the differential conductance at zero bias reflects the Kondo peak in the density of states.

temperatures. The expected peak is clearly resolved at a temperature $k_BT \simeq 0.05\Gamma$. This is substantially higher than the temperature, $k_BT \simeq 0.025\Gamma$, at which the linear-response conductance peak has broadened unambiguously (+10%) over the minimum width. The peak in the nonlinear differential conductance is therefore likely

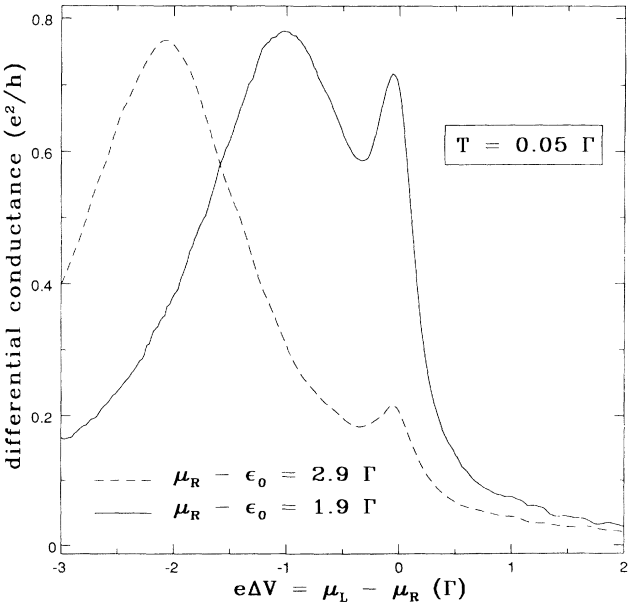

FIG. 9. Differential conductance $e\,dJ/d\Delta\mu$ vs applied bias for $\mu_R = 1.9$ (solid curve) and $\mu_R = 2.9$ (dashed curve) at $k_BT = 0.05$. Zero-bias peaks due to the Kondo effect appear for both curves despite the very different Kondo temperatures.

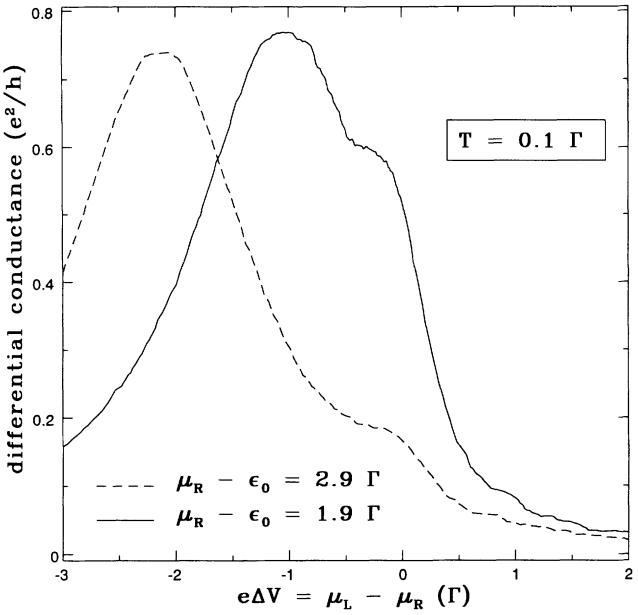

FIG. 10. Differential conductance $e\,dJ/d\Delta\mu$ vs applied bias for $\mu_R=1.9$ (solid curve) and $\mu_R=2.9$ (dashed curve) at $k_BT=0.1$. Both zero-bias peaks in Fig. 9 have become shoulders.

to be the first signal of the Kondo effect in transport through a quantum dot.

It is worth noting that the observability of the Kondo peak in the differential conductance depends only on the ratio k_BT/Γ, not on the Kondo temperature T_K. To demonstrate this, the differential conductance is plotted at different temperatures in Figs. 9 and 10, for level depths differing by Γ, and, consequently, Kondo temperatures differing by a factor of $\exp(\pi|\Delta\epsilon_0|/\Gamma)\simeq 23$. If the presence of a zero-bias peak depended on the Kondo temperature one would expect the peaks to wash out at temperatures differing by a factor of 23. Indeed, both the zero-bias peaks are clearly visible at $k_BT=0.05\Gamma$ (Fig. 9), but by $k_BT=0.1\Gamma$ (Fig. 10) *both* peaks have washed out. This behavior of the differential conductance reflects the temperature dependence of the Kondo peak in the density of states. While the final saturation of the density of states peak occurs at temperatures below the Kondo temperature $T_K\sim\exp(-\pi(\mu-\epsilon_0)/\Gamma)$, the temperature at which the Kondo peak first appears depends only on the coupling strength Γ. Since the peak first appears below $k_BT\simeq 0.1\Gamma$, the differential conductance develops a zero-bias peak just below this temperature.

III. DISCUSSION

A. Theoretical results

The most important result of this paper is a better qualitative and quantitative understanding of the low-temperature nonequilibrium properties of an Anderson impurity. The nonequilibrium characteristics, in particular the transport properties, follow from the form of the nonequilibrium density of states $\rho_\sigma(\omega)$. In this section, we discuss the main features of the density of states using both the results of the noncrossing approximation and other methods.[4,9,25]

The most obvious features in the low-temperature *equilibrium* density of states for an Anderson impurity with $\mu>\epsilon_0$ are the sharp peak at the chemical potential and the low, broad peak around the bare-level energy (Fig. 5). To understand these features it is useful to recall how, at equilibrium, the density of states depends on the eigenstates of the system. At $T=0$, the density of states, $\rho_\sigma(\omega)=-(1/\pi)\,\mathrm{Im}G^r_\sigma(\omega)$, involves transitions from the N-particle ground state to all $(N+1)$- or $(N-1)$-particle states. Since the correlated ground state of an Anderson impurity has a finite amplitude to have an empty site, the density of states includes a narrow peak due to transitions from the N-particle ground state to the ground state with one more or one less electron. By definition the ground-state energies differ by the chemical potential, so this Kondo peak in the density of states occurs at the chemical potential. The weight of the Kondo peak is small, however, since the probability that the site is unoccupied in the ground state is much less than 1. The remaining weight, associated with transitions to excited states, forms the low, broad peak around the bare-level energy ϵ_0. For finite interaction energy U, there is an additional broad feature in the density of states near ϵ_0+U; this feature does not appear in Fig. 5 because of the limit $U\to\infty$.

Out of equilibrium, there is no true ground state of the system, but quantum fluctuations still produce a finite probability of an empty site. As at equilibrium, these fluctuations involve electrons hopping between the site and states in the leads near each chemical potential.[4,9] The $N\to N+1$ and $N\to N-1$ transitions which determine the nonequilibrium density of states therefore include some excitations which change the system only by adding an electron or hole near one of the chemical potentials. These low-energy transitions produce the Kondo peaks near each chemical potential in the nonequilibrium density of states.

Unlike equilibrium, the configurations of the system out of equilibrium are not true eigenstates, but have a finite lifetime τ. The energies of transitions are therefore broadened by $\hbar/\tau$, and all features in the density of states are broadened an equivalent amount. This is the origin of the suppression of the Kondo peaks out of equilibrium (Fig. 5). The finite lifetime is due to real processes in which an electron is transferred from the higher-chemical-potential lead to the lower-chemical-potential one. An estimate of this lifetime can be obtained from straightforward perturbation theory in the coupling strength. One assumes that the site is initially occupied by an electron of spin σ and calculates the decay rate using the golden rule.[41] The only complication is that, at $T=0$, the lowest-order, energy-conserving process involves two separate tunneling events (the site electron hops out, and another electron hops in), and therefore occurs at $O(V^4)$. Allowing for two, possibly nondegenerate spin states, we find

$$\frac{1}{\tau_\sigma}=\frac{1}{\hbar}\sum_{A=L,R}\Gamma_\sigma^A(\epsilon_\sigma)[1-f_A(\epsilon_\sigma)]+\frac{1}{4\pi\hbar}\sum_{\substack{A,B=L,R\\ \sigma'}}\int_{-\infty}^{\infty}d\epsilon\left[\frac{1}{(\epsilon_\sigma-\epsilon+i\eta)^2}+\frac{1}{(\epsilon_\sigma-\epsilon-i\eta)^2}\right]$$
$$\times\{\Gamma_\sigma^A(\epsilon)\Gamma_{\sigma'}^B(\epsilon-\epsilon_\sigma+\epsilon_{\sigma'})[1-f_A(\epsilon)]f_B(\epsilon-\epsilon_\sigma+\epsilon_{\sigma'})\}\ . \quad (42)$$

For a deep level, $\epsilon_0<\mu_L,\mu_R$, so at zero temperature and for constant Γ, Eq. (42) reduces to

$$\frac{1}{\tau_\sigma}=\frac{1}{2\pi\hbar}\sum_{\substack{A,B=L,R\\ \sigma'}}\Gamma_\sigma^A\Gamma_{\sigma'}^B\theta(\mu_B-\mu_A+\epsilon_\sigma-\epsilon_{\sigma'})$$
$$\times\frac{\mu_B-\mu_A+\epsilon_\sigma-\epsilon_{\sigma'}}{(\mu_A-\epsilon_\sigma)(\mu_B-\epsilon_{\sigma'})}\ , \quad (43)$$

which explicitly shows that the lifetime is only nonzero for finite bias, or finite level splitting. The results of the noncrossing approximation are consistent with a broadening of Kondo peaks by the inverse of the nonequilibrium lifetime $\hbar/\tau_\sigma$. In effect, $\hbar/\tau_\sigma$ is a new cutoff energy for the logarithmic scaling of interactions in the Kondo problem.[38]

B. Relation to experiment

Since a quantum dot weakly coupled to its lead *is* an Anderson impurity, the results of the previous sections have practical significance. Specifically, at sufficiently low temperatures, transport through a quantum dot will be dominated by the Kondo effect. We discuss the practical requirements for the Kondo effect to be observed in quantum dots, and suggest possible experiments.

There are two general classes of transport experiments to study the Kondo effect in quantum dots: linear response and nonlinear response. While detection of the Kondo peak in the density of states is possible in the linear-response conductance, the nonlinear conductance offers a clearer signature and one that persists to higher temperatures. Figures 6 and 7 indicate the appearance of the Kondo effect in linear response. The sweep of chemical potential indicated in the figures can be accomplished by sweeping the voltage of a separate gate which couples capacitively to the dot.[16] In fact, conductance peaks with Lorentzian tails have already been observed in transport through a quantum dot by this method.[21] The long tails of the peaks imply that coherent transport of electrons is taking place. However, so far no broadening of the conductance peaks at zero magnetic field has been observed down to $T\simeq 50$ mK. This is consistent with the prediction of the noncrossing approximation that noticeable broadening ($+10\%$) occurs by $k_BT\simeq 0.025\Gamma$, since the largest resonance width in the experiment is $\Gamma\sim 40$ μeV for which 10% broadening is not reached until $T\simeq 10$ mK.

The appearance of the Kondo effect in nonlinear response is shown in Figs. 8, 9, and 10. The sharp drop of the differential conductance around zero applied bias reflects the sharpness of the Kondo peak in the density of states.[3,4] Furthermore, the peak in the differential conductance persists to $k_BT\simeq 0.05\Gamma$ and therefore should be observable in existing quantum dots up to $T\simeq 20$ mK. The magnitude of this zero-bias peak is optimized by performing the differential-conductance measurement at the half-maximum point of the linear-response conductance peak (as we have done in Fig. 8).

An additional, striking signature of the Kondo effect in nonlinear response is the evolution of the peak in the differential conductance with magnetic field. From perturbation theory,[25] and from an equations-of-motion approach,[4,9] it can be shown that a finite magnetic field shifts the Kondo peaks in the nonequilibrium densities of states by the Zeeman energy, and consequently splits the peak in the differential conductance by twice the Zeeman splitting of the levels.

Unfortunately, the behavior of the differential conductance in a finite magnetic field is beyond the scope of the noncrossing approximation. Specifically, when the level degeneracy is broken, the noncrossing approximation produces, in addition to the peaks found by the other methods, spurious peaks in the density of states. These peaks are due to a false interaction of each level with itself, brought on by the neglect of vertex corrections. While self-interaction effects are unimportant in the large-N limit, for finite N the corrections can be significant. An extreme example is the noninteracting case $N=1$, where the noncrossing approximation incorrectly predicts a Kondo peak in the density of states. Because of this false self-interaction, the noncrossing approximation produces additional Kondo peaks at the chemical potentials for nondegenerate levels, and therefore is unreliable for transport properties in a magnetic field. Interestingly, the noncrossing approximation continues to produce reliable results in a magnetic field for thermodynamic quantities (e.g., magnetization[32]) which depend on the entire density of states and not just on the behavior near the Fermi surface.

IV. CONCLUSION

In summary, we have analyzed the low-temperature, nonequilibrium properties of an Anderson impurity in the limit of infinite on-site interaction. The model corresponds to a quantum dot, weakly coupled to two leads with different chemical potentials. The Kondo effect, which dominates transport through the impurity, is modified by two new energies present in nonequilibrium: the chemical-potential difference $\Delta\mu$, and the inverse of the dissipative lifetime $\hbar/\tau_\sigma$ (42). These energies are apparent in the nonequilibrium density of states, which we obtain via the noncrossing approximation. The chemical-potential difference appears in the density of states via the splitting of the Kondo peak into two peaks, one at each chemical potential. The amplitudes of these peaks are suppressed by dissipative processes in which an electron is transferred from the higher-chemical-potential lead to the lower-chemical-potential one.

Experimentally, we predict that the Kondo effect can be observed in transport through a quantum dot by either linear or nonlinear measurements. The emergence of the Kondo peak in the density of states at low temperatures will cause the linear-response conductance peaks vs gate voltage to broaden, shift, and increase in amplitude roughly logarithmically with decreasing temperature. For a symmetric structure the conductance amplitude will saturate at $2e^2/h$, the conductance of an open channel.[17,18] The clearest feature of the Kondo effect in linear response, however, is the broadening of the conductance peak, which is predicted to reach $+10\%$ below $k_B T \simeq 0.025\Gamma$, where Γ is the total coupling strength to the leads. In nonlinear response, the Kondo peak will produce a peak in the differential conductance around zero bias.[3] Since this nonlinear peak remains clearly defined for temperatures up to $k_B T \simeq 0.05\Gamma$, we believe it will be the most accessible signature of the Kondo effect in quantum dots.

ACKNOWLEDGMENTS

We thank Dan Cox, Roger Lake, and Patrick A. Lee for valuable discussions. Work at U.C.S.B. was supported by NSF Grant No. NSF-DMR90-01502 and by the NSF Science and Technology Center for Quantized Electronic Structures, Grant No. DMR 91-20007.

APPENDIX

In this appendix, we show that the noncrossing approximation is current conserving. Specifically, the current through the Anderson impurity can be expressed either as a current flowing from the left lead into the site or as a current flowing from the site into the right lead. Within the noncrossing approximation, these two expressions are equivalent.

The full expression for the current through the left (right) tunneling barrier, with no restriction on the relative couplings to the leads,[22] is

$$J_{L(R)} = +(-)\frac{ie}{\hbar}\sum_{\sigma}\int_{-\infty}^{\infty} d\omega\, \Gamma_{\sigma}^{L(R)}(\omega)\{[1-f_{L(R)}(\omega)]G_{\sigma}^{<}(\omega)+f_{L(R)}(\omega)G_{\sigma}^{>}(\omega)\}\ , \tag{A1}$$

where $G_{\sigma}^{\lessgtr}(\omega)$ are Fourier transforms of the physical-electron Green functions defined in (9). In the noncrossing approximation, these Green functions factorize into boson and fermion parts,

$$G_{\sigma}^{\lessgtr}(\omega) \overset{\text{NCA}}{=} \frac{i}{2\pi}\frac{Z_{Q=0}}{Z_{Q=1}}\int_{-\infty}^{\infty} d\omega' D^{\gtrless}(\omega')G_{f\sigma}^{\lessgtr}(\omega+\omega')\ . \tag{A2}$$

Since this factorization is an approximation, one can ask whether the two expressions for the current (A1) remain identical.

To show that current is conserved in the noncrossing approximation, we examine the difference $J_L - J_R$ between the currents flowing through the two tunneling barriers,

$$\begin{aligned} J_L - J_R = -\frac{e}{2\pi\hbar}\frac{Z_{Q=0}}{Z_{Q=1}}\sum_{\sigma}\sum_{L,R}\int_{-\infty}^{\infty} d\omega \int_{-\infty}^{\infty} d\omega' \Gamma_{\sigma}^{L(R)}(\omega)\{[1-f_{L(R)}(\omega)]D^{>}(\omega')G_{f\sigma}^{<}(\omega+\omega') \\ +f_{L(R)}(\omega)D^{<}(\omega')G_{f\sigma}^{>}(\omega+\omega')\}\ . \end{aligned} \tag{A3}$$

This expression is simplified by recognizing that the ω integration produces factors of the boson self-energies,

$$\begin{aligned} \Pi^{>}(\omega') &= \frac{1}{2\pi}\sum_{\sigma}\sum_{L,R}\int_{-\infty}^{\infty} d\omega\, \Gamma_{\sigma}^{L(R)}(\omega)f_{L(R)}(\omega)G_{f\sigma}^{>}(\omega+\omega')\ , \\ \Pi^{<}(\omega') &= -\frac{1}{2\pi}\sum_{\sigma}\sum_{L,R}\int_{-\infty}^{\infty} d\omega\, \Gamma_{\sigma}^{L(R)}(\omega)[1-f_{L(R)}(\omega)]G_{f\sigma}^{<}(\omega+\omega')\ . \end{aligned} \tag{A4}$$

The difference can therefore be written as

$$J_L - J_R = \frac{1}{2\pi}\frac{Z_{Q=0}}{Z_{Q=1}}\int_{-\infty}^{\infty} d\omega'[D^{>}(\omega')\Pi^{<}(\omega')-D^{<}(\omega')\Pi^{>}(\omega')]\ . \tag{A5}$$

The integrand vanishes because of the relation between the boson Green functions and self-energies (22),

$$D^{\lessgtr}(\omega) = D^{r}(\omega)\Pi^{\lessgtr}(\omega)D^{a}(\omega)\ . \tag{A6}$$

The noncrossing approximation therefore explicitly conserves current,

$$J_L = J_R\ . \tag{A7}$$

[1]For a review, see P. Fulde, J. Keller, and G. Zwicknagl, Solid State Phys. **41**, 1 (1988).

[2]For a review, see H. van Houten, C. W. J. Beenakker, and A. A. M. Staring, in *Single Charge Tunneling,* edited by H. Grabert and M. Devoret (Plenum, New York, 1992).

[3]S. Hershfield, J. H. Davies, and J. W. Wilkins, Phys. Rev. Lett. **67**, 3720 (1991); Phys. Rev. B **46**, 7046 (1992).

[4]Y. Meir, N. S. Wingreen, and P. A. Lee, Phys. Rev. Lett. **70**, 2601 (1993).

[5]D. Ephron, Y. Xu, and M. R. Beasley, Phys. Rev. Lett. **69**, 3112 (1992).

[6]D. C. Ralph and R. A. Buhrman, Phys. Rev. Lett. **69**, 2118 (1992).

[7]P. W. Anderson, Phys. Rev. **124**, 41 (1961).

[8]D. V. Averin and A. N. Korotkov, Zh. Eksp. Teor. Fiz. **97**, 927 (1990) [Sov. Phys. JETP **70**, 937 (1990)].

[9]Y. Meir, N. S. Wingreen, and P. A. Lee, Phys. Rev. Lett. **66**, 3048 (1991).

[10]C. W. J. Beenakker, Phys. Rev. B **44**, 1646 (1991).

[11]M. A. Reed, J. N. Randall, R. J. Aggarwal, R. J. Matyi, T. M. Moore, and A. E. Wetsel, Phys. Rev. Lett. **60**, 535 (1988).

[12]P. L. McEuen, E. B. Foxman, U. Meirav, M. A. Kastner, Y. Meir, N. S. Wingreen, and S. J. Wind, Phys. Rev. Lett. **66**, 1926 (1991).

[13]A. T. Johnson, L. P. Kouwenhoven, W. de Jong, N. C. van der Vaart, C. J. P. M. Harmans, and C. T. Foxon, Phys. Rev. Lett. **69**, 1592 (1992).

[14]R. C. Ashoori, H. L. Stormer, J. S. Weiner, L. N. Pfeiffer, S. J. Pearton, K. W. Baldwin, and K. W. West, Phys. Rev. Lett. **68**, 3088 (1992).

[15]H. van Houten and C. W. J. Beenakker, Phys. Rev. Lett. **63**, 1893 (1989).

[16]U. Meirav, M. A. Kastner, and S. J. Wind, Phys. Rev. Lett. **65**, 771 (1990).

[17]L. I. Glazman and M. E. Raikh, Pis'ma Zh. Eksp. Teor. Fiz. **47**, 378 (1988) [JETP Lett. **47**, 452 (1988)].

[18]T. K. Ng and P. A. Lee, Phys. Rev. Lett. **61**, 1768 (1988).

[19]By particle-hole symmetry at finite U, one expects the conductance peak near ϵ_0+U to shift to lower chemical potential with decreasing temperature.

[20]N. E. Bickers, Rev. Mod. Phys. **59**, 845 (1987).

[21]E. B. Foxman, P. L. McEuen, U. Meirav, N. S. Wingreen, Y. Meir, P. A. Belk, N. R. Belk, M. A. Kastner, and S. J. Wind, Phys. Rev. B **47**, 10 020 (1993).

[22]Y. Meir and N. S. Wingreen, Phys. Rev. Lett. **68**, 2512 (1992).

[23]S. Barnes, J. Phys. F **6**, 1375 (1975); **7**, 2637 (1977).

[24]P. Coleman, Phys. Rev. B **29**, 3035 (1984); **35**, 5072 (1987).

[25]Nonequilibrium can be addressed via low-order perturbation theory in the hopping, provided the proper unperturbed occupations are taken for the site [N. Sivan, N. S. Wingreen, and Y. Meir (unpublished)].

[26]L. V. Keldysh, Zh. Eksp. Teor. Fiz. **47**, 1515 (1965) [Sov. Phys. JETP **20**, 1018 (1965)].

[27]C. Caroli, R. Combescot, P. Nozieres, and D. Saint-James, J. Phys. C **4**, 916 (1971).

[28]T. Matsubara, Prog. Theor. Phys. **14**, 351 (1955).

[29]M. Gell-Mann and F. Low, Phys. Rev. **84**, 350 (1951).

[30]G. D. Mahan, *Many-Particle Physics,* 2nd ed. (Plenum, New York, 1990).

[31]Equation (14) requires that $\langle \mathbf{O} \rangle_{Q=0}=0$. Since $Q=0$ corresponds to the case where there is no Anderson impurity, all the operators involving the site will satisfy this condition.

[32]D. L. Cox, Phys. Rev. B **35**, 4561 (1987).

[33]G. D. Mahan, *Many-Particle Physics* (Ref. 30), pp. 124–125. In the Dyson equations, additional terms involving the lesser and greater boson and fermion Green functions for the uncoupled site are found to be zero. This reflects the loss of memory of the initial occupation of the site in the coupled system.

[34]It would not be correct in (23) to include self-energies for the Green functions in the leads. Such self-energies include a fermion-boson loop which contributes an extra, unwanted factor of $\exp(-i\beta\lambda)$.

[35]The use of Anderson's model always requires a high-energy cutoff, either the bandwidth W, or the Coulomb energy U. P. W. Anderson, *Basic Notions of Condensed Matter Physics* (Benjamin-Cummings, Menlo Park, 1984), p. 193.

[36]D. L. Cox, Ph.D. thesis, Cornell University, 1985.

[37]P. J. Davis, in *Handbook of Mathematical Functions,* edited by M. Abramowitz and I. Stegun (Dover, New York, 1968), pp. 258–259.

[38]J. Kondo, Prog. Theor. Phys. **32**, 37 (1964).

[39]Y. Kuramoto and H. Kojima, Z. Phys. B **57**, 95 (1984); E. Müller-Hartmann, *ibid.* **57**, 281 (1984).

[40]D. C. Langreth, Phys. Rev. **150**, 516 (1966).

[41]L. I. Schiff, *Quantum Mechanics* (McGraw-Hill, New York, 1949), pp. 189–199.

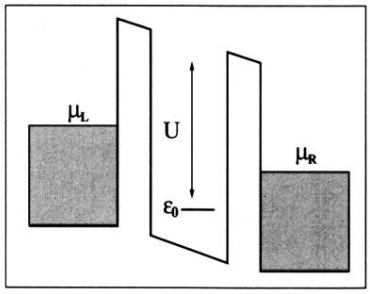

FIG. 1. Schematic band diagram of a quantum dot coupled via tunneling barriers to two leads with different chemical potentials. At zero magnetic field, the energy level ϵ_0 on the quantum dot will be spin degenerate, and a large Coulomb interaction energy U will prevent double occupancy.